iScience, Volume *24*

Supplemental information

Safety and improved efficacy signals following gene therapy in childhood blindness caused by *GUCY2D* mutations

Samuel G. Jacobson, Artur V. Cideciyan, Allen C. Ho, Igor V. Peshenko, Alexandra V. Garafalo, Alejandro J. Roman, Alexander Sumaroka, Vivian Wu, Arun K. Krishnan, Rebecca Sheplock, Sanford L. Boye, Alexander M. Dizhoor, and Shannon E. Boye

Supplemental Information

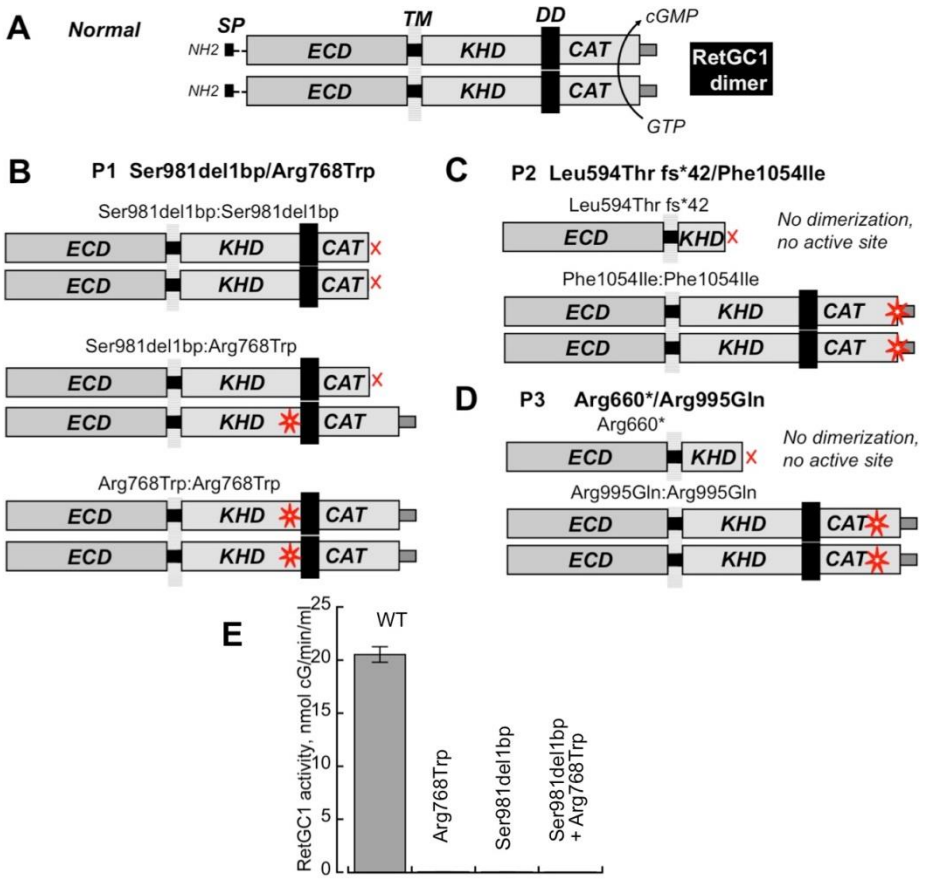

Figure S1: RetGC1 dimer combinations that can be produced by the *GUCY2D* alleles in the patients. Related to Figure 1. (A) The schematics of the normal RetGC1 primary structure and its catalytically active dimer; SP- the removable N-terminal signal peptide, ECD- extracellular domain, TM- transmembrane fragment, KHD- kinase homology domain, DD- dimerization domain, CAT- catalytic domain (Garbers, 1999). RetGC1 becomes catalytically active only as a dimer (Yang et al., 1997), when the catalytic domains of the two subunits form a common active site converting GTP to cGMP (Liu et l., 1997). (B) In P1 (Table 1), the Ser981del1bp frame-shift truncates the C-terminal portion of the catalytic domain, but the products of both alleles harbor the normal dimerization domain and hence can produces homodimers Ser981del1bp:Ser981del1bp or Arg768Trp:Arg768Trp and a heterodimer Ser981del1bp: Arg768Trp. (C) One of the two LCA alleles in the patient P2, Phe1054Ile, retains both the dimerization domain and the catalytic domain. The Leu594Thr fs42* RetGC1 coded by the second LCA allele has a truncated kinase homology domain and lacks both the dimerization and the catalytic domains altogether. Hence, this RetGC1 mutant cannot create the active site and likely fails to dimerize, neither as a homodimer nor as a heterodimer. (D). In P3, also only one of the two *GUCY2D* LCA alleles, Arg995Gln, can form a homodimer Arg995Gln: Arg995Gln. The second allele product, Arg660*, is truncated in the middle of the kinase homology domain, hence it lacks the dimerization and the catalytic domains and would be unable to dimerize and form the active site. *Asterisks* indicate position of the mutations in the primary structure of the polypeptides. (E) HEK293 cells co-transfected with RetGC1 cDNAs coding for the two LCA allele products in P1 do not produce active enzyme. RetGC activity was assayed in the presence of 20 µM GCAP1.

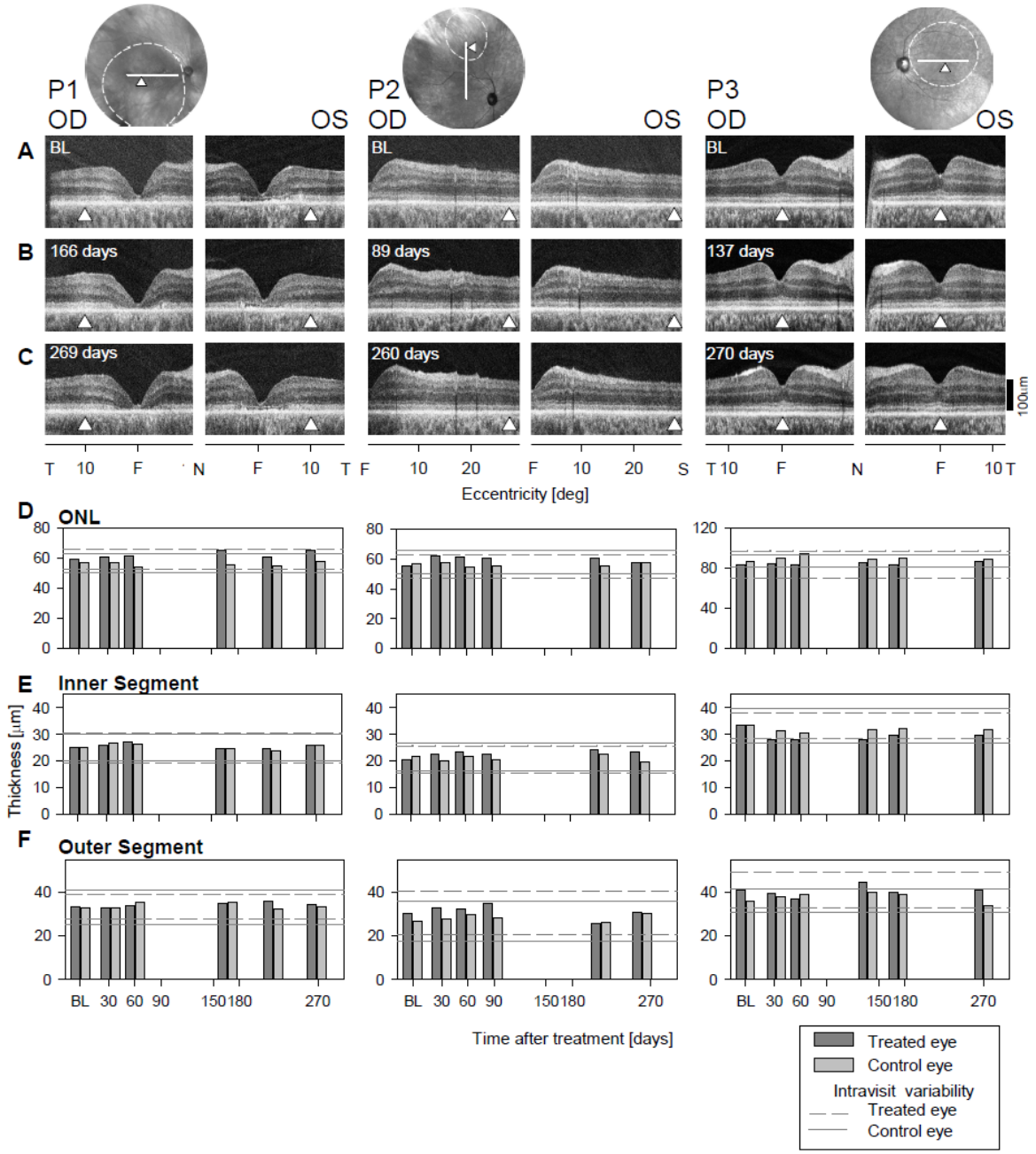

Figure S2: Quantitation of the photoreceptor sublayers in the patients at Baseline and post-operative visits spanning 9 months. Related to Figure 2. Representative OCT scans at (A) Baseline, (B) visit 3 and (C) visit 5 after the surgery. Above the scans are near-infrared fundus images of the treated eyes with site of bleb (injection location) marked (delimited by dashed line). White lines on the fundus images represent the position of the OCT scan. The white up-triangle along the line on the fundus images and on the eccentricity axes of the scans show the location selected for quantitation of photoreceptor layers in D-F. (D) Bar graphs are a measurement of ONL (outer nuclear layer), (E) IS (inner segment), and (F) OS (outer segment) thickness at baseline and at five visits after surgery for the treated eye (dark gray bar) and control eye (light gray bar). Dashed and solid black lines delimit intravisit variability in the treated and untreated eye, respectively.

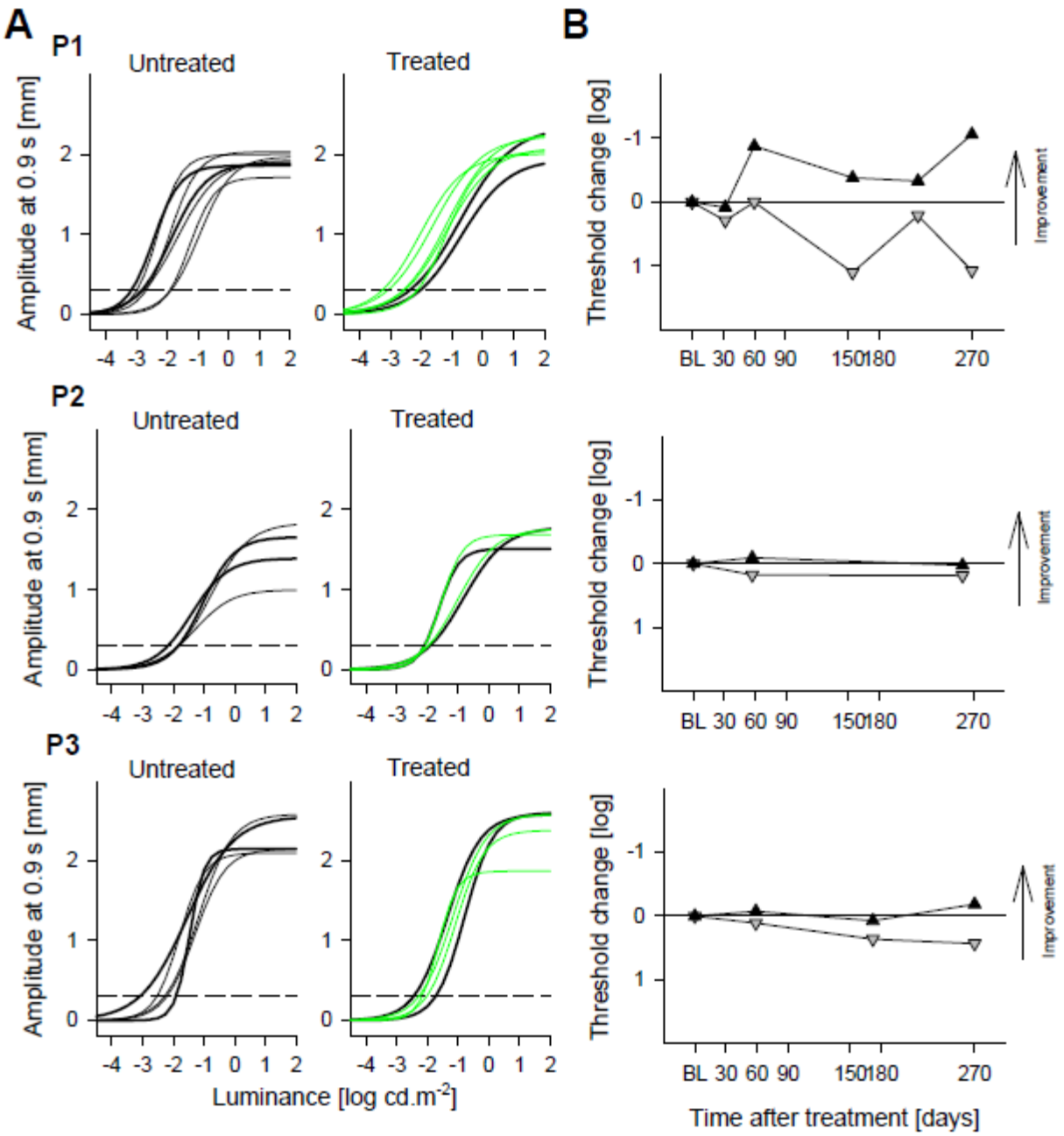

Figure S3: Dark-adapted pupillary light reflexes in the patients at baseline and post-operative visits spanning 9 months. Related to Figure 3. (A) Non-linear functions best fit to pupillary response amplitudes measured at 0.9 s after the start of 1 s long red stimuli over a 6 log unit dynamic range of luminances presented to dark-adapted eyes. Thicker lines represent the pre-treatment time points, thinner black and green lines represent the post-treatment time points in untreated and treated eyes, respectively. Horizontal dashed lines demarcate criterion amplitude of 0.3 mm used to define response thresholds. (B) Change in response threshold from average pre-treatment values. Black up-triangles are treated eyes; gray down-triangles are untreated control eyes.

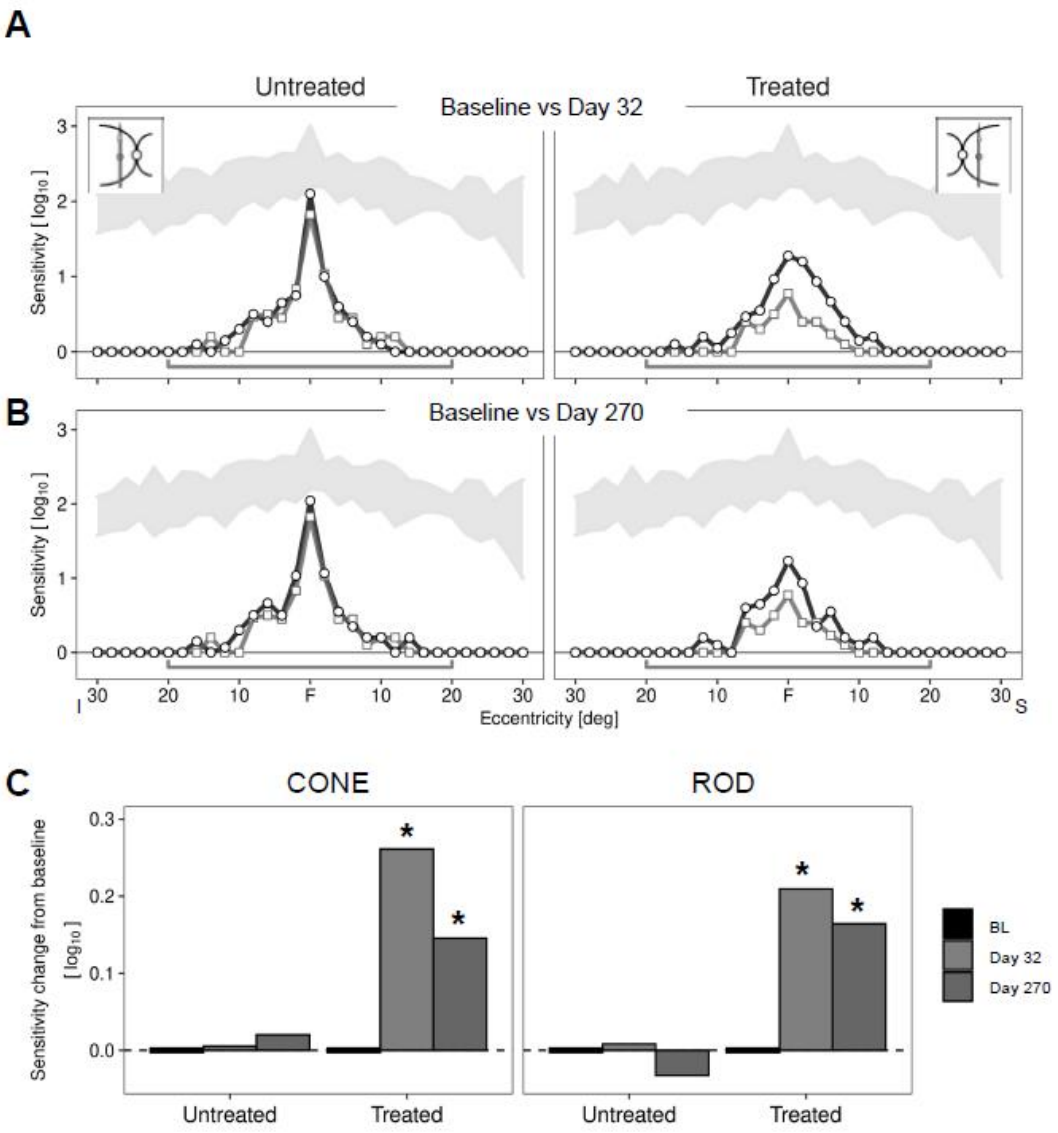

Figure S4. Cone and rod function at baseline and post-op visits in P3. Related to Figure 4. (A) Light-adapted (600 nm stimulus) sensitivity profiles across the vertical meridian in untreated (left panel) and treated (right panel) eyes at baseline (symbols connected by gray lines) and post-op day 32 (symbols connected by black lines) visits in P3. Normal data, shaded area ±2 SD from mean. (B) Light-adapted profiles comparing baseline and 270 days post-op visit data in P3. Plots and symbols as in A. F, fixation; I, inferior, S, superior visual field; bracket below profiles represents the data averaged and plotted for the horizontal profile. Data from vertical profiles within the central 40º were also averaged and plotted in C. (C) Sensitivity changes (average of horizontal and vertical profiles across central 40^{o}) are shown as bars for untreated and treated eyes. Left panel: light-adapted 600 nm data. Right panel: dark-adapted 500 nm data. All dark-adapted 500 nm sensitivities were rod-mediated. Asterisks on the treated eye bars indicate when interocular differences with respect to baseline were significantly different than zero (α=0.05, eye/visit interaction term in a linear model).

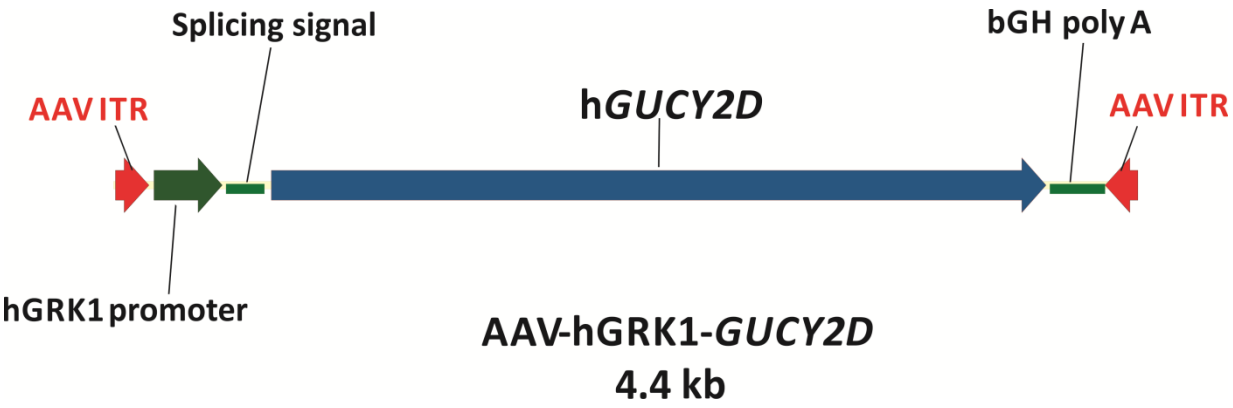

Figure S5. Schematic diagram of the gene therapy vector. Related to Table 1. AAV ITR= Adeno-associated virus type 2 inverted terminal repeat; hGRK1= human rhodopsin promoters (Khani et al. 2007); splicing signal= SV40 splice donor, splice acceptor sites; h*GUCY2D*= full coding region of human guanylate cyclase 1; bGH polyA= bovine growth hormone poly-adenylation signal

Table S1. Schedule of Study Visits. Related to Table 1.

Visit:	*Pre-therapy*		*Days*											*Years*	
	Screening	Baseline	1	2	3	4-7	8-14	30	60	90	180	270	365	1.5	2
Informed consent/assent	■														
LCA genetic testing (if needed)	■														
Medical and surgical history	■														
Physical examination	■														
Electrocardiogram	■														
Pregnancy test	■	■						■							
Vital signs measurements	■	■	■	■	■	■	■	■	■	■	■	■	■	■	■
Study agent administration			■												
Hematology, chemistry, urinalysis	■	■				■		■					■		■
Ophthalmic exam	■	■		■	■	■	■	■	■	■	■	■	■	■	■
Best corrected visual acuity	■	■		■	■	■	■	■	■	■	■	■	■	■	■
Full-field stimulus testing	■	■			■		■	■	■	■	■	■	■	■	■
Fundus imaging	■	■		■	■			■	■	■	■	■	■	■	■
Optical coherence tomography	■							■	■	■	■	■	■	■	■
Pupillometry	■	■						■	■	■	■	■	■	■	■
Oculomotor instability	■	■						■	■	■	■	■	■	■	■
Questionnaire		■						■		■	■		■	■	■
Adverse event recording	■	■	■	■	■	■	■	■	■	■	■	■	■	■	■

Note: Electroretinography (ERG) was not performed due to the facts that ERGs are non-detectable in most of these patients and nystagmus can make recording and interpretation difficult.
Note: Dosing and cohort information is as follows:
Part A: Dose Escalation
Part B: Patients will be treated with the maximum tolerated dose or the maximum administered dose based on Part A.
Total enrollment will be approximately 15 patients.
Cohorts 1-4: patients ≥18 years old
Cohort 5: patients ≥6 years old and <18 years old

Table S2. Ocular Adverse Events. Related to Table 1.

Description of adverse event	No. of patients experiencing event (n=3)	Intensity
Discomfort	3	Mild
Subconjunctival hemorrhage	3	Mild
Hypotony	2	Mild
Vitreous cells	1	Mild
Steroid induced ocular hypertension	1	Mild
Retinal hole	1	Mild

TRANSPARENT METHODS

REGULATORY APPROVALS AND OVERSIGHT

The open label clinical trial, registered on ClinicalTrials.gov (NCT03920007), is being performed at Scheie Eye Institute of the University of Pennsylvania (UP) and Wills Eye Institute (WEI) of Thomas Jefferson University Hospital. The trial protocol was reviewed and accepted by the United States Food and Drug Administration (Investigational New Drug application IND 18659). Approvals were obtained from the Institutional Review Boards and Institutional Biosafety Committees of UP and WEI. A Data and Safety Monitoring Committee oversees the trial. The tenets of the Declaration of Helsinki were followed. Informed consent was obtained from the participants.

METHOD DETAILS

The gene therapy vector (Figure S5). The AAV5-*GUCY2D* vector comprises the human rhodopsin kinase promoter (Khani et al.,2007), followed by the human *GUCY2D* coding sequence (accession # NM_000180.4) and a poly adenylation signal derived from bovine growth hormone, all flanked by AAV2 inverted terminal repeats and contained within AAV5 capsid. Virus was manufactured under good manufacturing practices (GMP) and purified as previously described (Nass et al., 2017).

Molecular diagnosis. *GUCY2D* mutations in the patients were certified by CLIA (Clinical Laboratory Improvement Amendments) approved molecular laboratories.

Surgical procedure. Three port pars plana vitrectomy (core and peripheral; intravitreal triamcinolone was used) was performed and a posterior vitreous detachment was induced. The subretinal injection needle (41-gauge) was guided to the region around the superior vascular arcades and the surgeon placed a retinotomy within the boundaries of the arcades (MicroDose Injection Kit, MedOne Surgical, Inc). The study drug was injected slowly to form a subretinal bleb in the macula. After study drug administration, the fundus was examined for any retinal breaks. A partial air-fluid exchange was performed. Sclerotomy sites were inspected for leakage and no sclerotomies required suturing. A normal intraocular pressure was verified. Triamcinalone acetonide (20mg in 0.5mL) was injected periocularly. Patients took oral prednisone (dose at investigator discretion, but a maximum dose of 1mg/kg up to 80mg) daily starting the day before surgery through the second day following surgery. Prednisolone 1% drops and trimethoprim and polymyxin B drops were also administered to the study eye four times per day starting the day after surgery through day 9.

Safety evaluations. Ocular safety was assessed with standard eye examinations at two baseline visits, and daily for the first 14 days after treatment and at 5 visits post-treatment spanning 9 months. OCT was performed to assess retinal integrity during the pre- and post-treatment evaluations. Systemic safety at baseline and post-operative visits was assessed with physical examinations, routine hematology, serum chemistry, coagulation parameters, and urinalysis. To document fundus appearance, photographs (using an infrared camera to avoid excess visible light exposure) were taken at baseline and at post-treatment visits.

Visual function and retinal structure. Visual function was measured using ETDRS visual acuity (Ferris et al., 1982) in two of the patients. One patient's severe visual disability precluded use of standard ETDRS methods and the Berkeley Rudimentary Vision Test was used (Bailey et al., 2012). Dark-adapted chromatic full-field stimulus testing (FST) was performed with short- (blue) and long-wavelength (red) stimuli (200 ms duration) (Jacobson et al., 2017; Roman et al., 2007) Dark-adapted transient pupillary light reflexes were performed with red (1 s duration) full-field stimuli (Charng et al., 2017; Krishnan et al.,

2020). In each patient, baseline data were available from screening and baseline pre-treatment visits; post-treatment data were obtained up to 9 months after surgery.

For FST, the dependent variable was visual threshold expressed in $\log_{10}$ phot-cd m^{-2}. Multiple measurements (median n=18) were obtained for both conditions (blue and red) at each visit. Linear models were used separately for each condition with treatment-by-visit interactions as fixed effects. The treatment factor had two levels (treated and untreated eyes), and the visit factor had 5 or 6 levels (baseline and subsequent study visits). The visits where the interactions were significant (α=0.05) are marked with asterisks (Figure 3), indicating where the interocular difference was significantly different than the one at baseline, and 95% confidence intervals for the visit means (±2 SEM) are shown in brackets. In these instances the treated eye showed better relative performance than the untreated.

For visual acuity, ETDRS and tumbling E charts read from left-to-right, and right-to-left were used in each eye to attempt to minimize learning effects. 5 to 8 independent acuity estimates were obtained pre-treatment on different days, 2 to 3 estimates were obtained post-treatment. Comparisons were performed between all available pre-treatment and post-treatment samples at month 9 (two sample, 2-tailed t-test, α=0.05). The dependent variable was the Minimum Angle of Resolution expressed in $\log_{10}$ (logMAR). Levels of change from baseline in logMAR and in ETDRS equivalent lines (no change, 3 lines improvement or decrease, these corresponding to ±0.3 logMAR changes; Figure 4) enabled comparison with other clinical trials of retinal degenerations that used ETDRS as an outcome (Sieving et al., 2006).

Chromatic light-adapted (600 nm) and dark-adapted (500 and 650 nm) sensitivity profiles were performed with a modified automated perimeter and using published methods (Roman et al., 2005; Matsui et al., 2015; Jacobson et al., 1986). A comparison of sensitivity changes from baseline (averaged over horizontal and vertical profiles within the central 40^0, Fig. 5) was performed as described for FST, with visit factor having three levels (baseline, Day 32 and Day 270), separately for 500- and 600 nm data.

Retinal structure was assessed by cross-sectional imaging using spectral domain optical coherence tomography (OCT; RTVue-100, Optovue Inc., Fremont, CA) (Jacobson et al., 2013; Jacobson et al., 2017; Sumaroka et al., 2016). The OCT images were recorded routinely in the macula and extramacular retina of each eye of the patients. Scans at post-operative visits were compared by observation with those at baseline; measurements were also made of outer nuclear layer (ONL), inner segment (IS) and outer segment (OS) thicknesses. Post-acquisition processing of OCT data was performed with custom programs (MATLAB Release, 2020, MathWork, Natick, MA). Three 30°-wide B-scans composed of 1,019 A-scans or longitudinal reflectivity profiles (LRPs) were selected from both eyes of each subject at each visit. All scans were aligned by straightening the major hyperreflective signal believed to originate near the interface between the basal aspect of the retinal pigment epithelium and Bruch's membrane; the foveola was identified manually as the maximum depression. Quantitative measurements of retinal laminae were performed after reduction of lateral sampling density by averaging seven neighbors (sampling bins were 0.2 degrees). Three retinal layers were identified and manually segmented with a computer-assisted algorithm using LRPs. The hyposcattering ONL was defined between the hyperscattering outer plexiform layer (OPL) and the maximum of hyperscattering outer limiting membrane (OLM); the foveal ONL thickness was defined as the distance between the internal limiting membrane and outer limiting membrane; IS length was defined as the distance between OLM peak and peak of IS/OS; and OS as distance between IS/OS peak and inner boundaries of RPE. From this segmentation, thickness of ONL, IS and OS layers were extracted. At selected eccentricities, single value of layer thickness represents the average of 3 measurements along the horizontal scan at 0.2-degree increments centered at the foveal pit, or 5 measurements with the same increment centered 10^o temporal and 28^o superiorly.

Biochemical studies. Human RetGC1 was expressed in HEK293 cells from a modified pRCCMV vector containing RetGC1 cDNA transfected using calcium-phosphate precipitation method and the membranes containing RetGC1 were isolated as previously described in detail (Peshenko et al., 2015). Mutations

were introduced in RetGC1 cDNA using ‘splicing by overlap extension’ site-directed mutagenesis *in vitro* or by using chemically synthesized fragments harboring the desired mutations to replace portions in the RetGC1 cDNA that harbored new restriction endonuclease sites not altering the encoded protein sequence (Peshenko et al., 2020). Recombinant human GCAP1 was expressed and purified as described (Peshenko et al, 2008) with modifications (Peshenko et al., 2019). Guanylyl cyclase activity was assayed using [alpha-^{32}P]GTP as a substrate (Peshenko et al., 2020; Peshenko et al., 2004) in the presence of 2 mM EGTA and 10 mM $MgCl_2$. [32P]cGMP was quantified using thin-layer chromatography and liquid scintillation counting as described previously (Peshenko et al., 2020).

Schedule of Study Visits. The schedule of study visits and the study activities performed at each visit are summarized in Table S1.

SUPPLEMENTAL REFERENCES

Bailey, I.L., Jackson, A.J., Minto, H., Greer, R.B., and Chu, M.A. (2012). The Berkeley rudimentary vision test. Optom. Vis. Sci. *89,* 1257-1264.

Charng, J., Jacobson, S.G., Heon, E., Roman, A.J., McGuigan, D.B., Sheplock, R., Kosyk, M.S., Swider, M., and Cideciyan, A.V. (2017). Pupillary light reflexes in severe photoreceptor blindness isolate the melanopic component of intrinsically photosensitive retinal ganglion cells. Invest. Ophthalmol. Vis. Sci. *58*, 3215-3224.

Jacobson, S.G., Voigt, W.J., Parel, J.M., Apáthy, P.P., Nghiem-Phu, L., Myers, S.W., and Patella, V. M. (1986). Automated light- and dark-adapted perimetry for evaluating retinitis pigmentosa. Ophthalmology *93*, 1604–1611.

Khani, S.C., Pawlyk, B.S., Bulgakov, O.V., Kasperek, E., Young, J.E., Adamian, M., Sun, X., Smith, A.J., Ali, R.R. and Li, T. (2007). AAV-mediated expression targeting of rod and cone photoreceptors with a human rhodopsin kinase promoter. Invest. Ophthalmol. Vis. Sci. *48*, 3954–3961.

Krishnan, A.K., Jacobson, S.G., Roman, A.J., Iyer, B.S., Garafalo, A.V., Héon, E., Cideciyan, A.V. (2020) Transient pupillary light reflex in CEP290- or NPHP5-associated Leber congenital amaurosis: latency as a potential outcome measure of cone function. Vision Res. *168*, 53-63.

Liu, Y., Ruoho, A.E., Rao, V.D., and Hurley, J.H. (1997). Catalytic mechanism of the adenylyl and guanylyl cyclases: modeling and mutational analysis. Proc. Natl. Acad. Sci. USA. *94,* 13414-13419.

Nass, S.A., Mattingly, M.A., Woodcock, D.A., Burnham, B.L., Ardinger, J.A., Osmond, S.E., Frederick, A.M., Scaria, A., Cheng, S.H. and O'Riordan, C.R. (2017). Universal method for the purification of recombinant AAV vectors of differing serotypes. Mol. Ther. Methods Clin. Dev. *9*, 33–46.

Peshenko, I.V., Moiseyev, G.P., Olshevskaya, E.V. and Dizhoor, A.M. (2004). Factors that determine Ca2+ sensitivity of photoreceptor guanylyl cyclase. Kinetic analysis of the interaction between the Ca2+-bound and the Ca2+-free guanylyl cyclase activating proteins (GCAPs) and recombinant photoreceptor guanylyl cyclase 1 (RetGC-1). Biochemistry *43*, 13796–13804.

Peshenko, I.V., Olshevskaya, E.V., and Dizhoor, A.M. (2008). Binding of guanylyl cyclase activating protein 1(GCAP1) to retinal guanylyl cyclase (RetGC1): the role of individual EF-hands. J. Biol. Chem. *283*, 21747-21757.

Peshenko, I.V., Olshevskaya, E.V., and Dizhoor, A.M. (2015). Evaluating the role of retinal membrane guanylyl cyclase 1 (RetGC1) domains in binding guanylyl cyclase-activating proteins(gCAPs). J. Biol. Chem. *290*, 6913-6924.

Peshenko, I.V., Cideciyan, A.V., Sumaroka, A., Olshevskaya, E.V.,Scholten, A., Abbas, S., Koch, K.W., Jacobson, S.G., and Dizhoor, A.M. (2019). A Gly86Arg mutation in the calcium-sensor protein GCAP1 alters regulation of retinal guanylyl cyclase and causes dominant cone-rod degeneration. J. Biol. Chem. *294*, 3476-3488.

Sumaroka, A., Matsui, R., Cideciyan, A.V., McGuigan, D.B.,3rd, Sheplock, R., Schwartz, S.B., and Jacobson, S.G. (2016). Outer retinal changes including the ellipsoid zone band in Usher syndrome 1B due to MYO7A mutations. Invest. Ophthalmol. Vis. Sci. *57*, OCT253-261.

Yang, R.B., and Garbers, D.L. (1997). Two eye guanylyl cyclases are expressed in the same photoreceptor cells and form homomers in preference to heteromers. J. Biol. Chem. *272*, 13738-13742.